Available online at www.sciencedirect.com
SCIENCE DIRECT
Solid State Communications 137 (2006) 326–331
solid state communications
www.elsevier.com/locate/ssc

Structure, magnetic, and transport properties of the Co-doped manganites $La_{0.9}Te_{0.1}Mn_{1-x}Co_xO_3$ $(0 \leq x \leq 0.25)$

G.H. Zheng, Y.P. Sun *, X.B. Zhu, W.H. Song

Key Laboratory of Materials Physics, Institute of Solid State Physics, Chinese Academy of Sciences, Hefei 230031, People's Republic of China

Received 8 September 2005; received in revised form 25 October 2005; accepted 2 November 2005 by C. Lacroix
Available online 18 November 2005

Abstract

The effect of Co doping at Mn-site on the structural, magnetic and electrical transport properties in electron-doped manganties $La_{0.9}Te_{0.1}Mn_{1-x}Coxo_3$ $(0 \leq x \leq 0.25)$ has been investigated. The room temperature structural transition from rhombohedra ($R\bar{3}C$) to orthorhombic (*Pbnm*) symmetry is found in these samples with $x \geq 0.20$ by the Rietveld refinement of X-ray powder diffraction patterns. All samples undergo the paramagnetic–ferromagnetic (PM–FM) phase transition. The Curie temperature T_C of these samples decreases and the transition becomes broader with increasing Co-doping level. The magnetization magnitude of Co-doping samples increases at low temperatures with increasing Co-doping level for $x \leq 0.15$ and decreases with increasing Co-doping content further. The metal–insulator (M–I) transitions observed in the sample with $x = 0$ are completely suppressed with Co doping, and the resistivity displays semiconducting behavior within the measured temperature region for these samples with $x > 0$. All results are discussed according to the changes of the structure parameters and magnetic exchange interaction caused by Co-doping. In addition, the different effects between the Co doping and Cu doping in the Mn site for the electron-doped manganites are also discussed.

PACS: 75.47.Lx; 71.30.+h; 75.30.Et

Keywords: A. Colossal magntoresistence; A. Perovskites; D. Electrical transport; D. Double exchange

1. Introduction

Mixed-valent manganites with perovskite structure have attracted considerable attention in recent years because of the observation of colossal magnetoresistence (CMR) and related physics phenomena. However, they are usually hole-doped manganites $La_{1-x}A_xMnO_3$ (Ln = La–Tb, and A = Ca, Sr, Ba, Pb, etc.) and have a mixed-valence state of Mn^{3+}–Mn^{4+} [1–4]. Recently, electron-doped compounds in which La was substituted by tetravalent ion such as Ce^{4+}, Te^{4+} and Zr^{4+} have been reported by some research groups [5–9]. These investigations also suggest that the CMR behavior probably occurs in the systems with the mixed-valence state of Mn^{2+}–Mn^{3+}.

It is well known that doping at Mn sites in perovskite oxides is very efficient to change their physical properties due to the core role of Mn ions in manganites. The doping effect at Mn sites of transitional elements has been undertaken extensively in the $LaMnO_3$ and the hole-doped $La_{1-x}A_xMnO_3$ (A = Ca, Sr, Ba, Pb, etc.) compounds [10–15]. Among all doping at Mn sites with transitional elements in perovskite-structure manganites, the Co doping is more remarkable since Co ion has three kinds of spin states, i.e. low spin (LS), intermediate spin (IS) and high spin (HS), resulting from the fact that the crystal field splitting (10Dq) of the Co3d states (E_{ef}) and Hund's rule coupling energy (E_{ex}) are comparable for the cobaltites. On the other hand, the valence state of cobalt ions incorporated into manganese-based perovskite oxides has also been one of most studied topics in many papers [16–20]. However, these results concerning about the influence of Co-doping on the properties of manganites are very controversial. Several authors think that Co ion incorporated into manganites is in Co^{3+} and Co doping will destroy the ferromagnetic (FM) order [13]. X-ray absorption spectroscopy (XAS) spectrum of $LaMn_{0.85}Co_{0.15}O_3$ [10] is found to be almost identical to that of the system $La_{0.80}Ca_{0.20}MnO_3$. These results show that the charge redistribution (CR) $Mn^{3+} + Co^{3+} \rightarrow Mn^{4+} + Co^{2+}$ occurs in the Co-doped manganese perovskites $LaMn_{0.85}Co_{0.15}O_3$ and then this system becomes Mn^{3+}–Mn^{4+} mixed valent. The X-ray

* Corresponding author. Tel.: +86 551 559 1436; fax: +86 551 559 1434.
E-mail address: ypsun@issp.ac.cn (Y.P. Sun).

0038-1098/$ - see front matter © 2005 Elsevier Ltd. All rights reserved.
doi:10.1016/j.ssc.2005.11.003

photoelectron spectroscopy (XPS) measurements of the $La_{0.7}Ba_{0.3}Mn_{1-x}Co_xO_3$ [19] and $Pr_{0.5}Ca_{0.5}Mn_{0.95}Co_{0.05}O_3$ [20] perovskites have also got the same results. These results unambiguously indicate that the $Co^{2+}+Mn^{4+}$ ionic configuration is more stable than the $Co^{3+}+Mn^{3+}$ one, due to the CR process of $Mn^{3+}+Co^{3+}\rightarrow Mn^{4+}+Co^{2+}$. The NMR[21]data also provide an evidence for the existence of Co^{2+} and Mn^{4+} ions in the FM $La(Mn_{0.5}Co_{0.5})O_3$. The CR process and the appearance of the Co^{2+} ions are very important and have to be taken into account in the analysis of the magnetic and electrical properties of Co-substituted manganites. In the present work, we investigate the effect of Co doping at Mn-site on structural, magnetic and electrical transport properties in the electron-doped manganites $La_{0.9}Te_{0.1}Mn_{1-x}Co_xO_3$ ($0\leq x\leq 0.25$). At the same time, the different effects between the Co doping and Cu doping in the Mn site in electron-doped manganites are also discussed.

2. Experimental

A series of ceramic samples of $La_{0.9}Te_{0.1}Mn_{1-x}Co_xO_3$ ($0\leq x\leq 0.25$) were synthesized by a conventional solid-state reaction method in air. The powders mixed in stoichiometric compositions of high-purity La_2O_3, TeO_2, MnO_2 and Co_2O_3 were ground, fired in air at 700 °C for 24 h. The obtained powders were ground, pelletized, and sintered at 1050 °C for 24 h with three intermediate grindings, and finally, the furnace was cooled down to the room temperature. The structure and lattice constant were determined by powder X-ray diffraction (XRD) using Cu K_α radiation at the room temperature. The resistance using the standard four-probe method was measured in a commercial Physical Property Measurement System (PPMS) ($1.9\ K\leq T\leq 400\ K$, $0\ T\leq H\leq 9\ T$) from 5 to 350 K. The magnetic measurements were carried out with a Quantum Design superconducting quantum interference device (SQUID) MPMS system ($1.9\ K\leq T\leq 400\ K$, $0\ T\leq H\leq 5\ T$).

3. Results and discussion

X-ray powder diffraction (XRD) at the room temperature shows that all samples are single phase with no detectable secondary phases. XRD patterns of these samples with $x=0$, 0.05, 0.10 and 0.15 can be indexed by a rhombohedral lattice with the space group $R\bar{3}C$. While XRD patterns of these samples with $x=0.20$ and 0.25 can be indexed by an orthorhombic lattice with the space group *Pbnm*. The structural parameters are refined by the standard Rietveld technique [22]. Based on the consideration of low R_p values as shown in Table 1, the fitting between the experimental spectra and the calculated values is considered to be very good. The experimental and calculated XRD patterns for these samples with $x=0$ and 0.20 are shown in the Fig. 1 (a) and (b), respectively. It can be seen that the crystal structure changes from a rhombohedral phase ($R\bar{3}C$, $Z=2$, $x\leq 0.15$) to an orthorhombic phase (*Pbnm*, $Z=4$, $x\geq 0.20$) for the samples $La_{0.9}Te_{0.1}Mn_{1-x}Co_xO_3$ ($0\leq x\leq 0.25$). To describe the ion match between A and B ions in the perovskite structure compound ABO_3, a geometrical quantity, tolerance factor t is usually introduced and t is defined as $t=(r_A+r_O)/\sqrt{2}(r_B+r_O)$, where r_i (i = A, B, or O) represents the average ionic size of each element. As t is close to 1, the cubic perovskites structure is expected to form. As t decreases, the lattice structure transforms to rhombohedral ($R\bar{3}C$), and then to the orthorhombic (*Pbnm*) structure. For the current investigated samples, the average ionic radius of A-site is fixed. Therefore, the lattice distortion observed is caused by the partial replacement of Mn by Co. Departure from the average radius $R(Mn_{av})$ of Mn ions at the dopant site would subject the neighboring Mn–O bonds to a centric push or pull. For the low concentration $0\leq x\leq 0.15$, the decrease of the average Mn–O–Mn bond angle and increase of Mn–O bond length are observed. The departure from the average radius of Mn ions at the dopant site subjects the neighboring Mn–O bonds to a centric pull. Only a bigger ion at the dopant site can compress some Mn–O–Mn bonds and result in decreasing the average Mn–O–Mn bond angle. However, for $x>0.15$, the average Mn–O–Mn bond angle increases and the Mn–O bond length decreases. Only when the ion radius at the dopant site is smaller than the average Mn radius, will the neighboring Mn–O bonds stretch, resulting in an increase of the average Mn–O–Mn bond angle. We have calculated $R(Mn_{av})$, which is defined as the average radii for Mn^{3+} and Mn^{2+} ions in the ratio 90:10 in $La_{0.9}Te_{0.1}MnO_3$ compounds, using standard ionic radii with values 0.83 Å for Mn^{2+} and 0.65 Å for Mn^{3+} in perovskite-structure manganites, respectively. The average radius of Mn ion $R(Mn_{av})$ is calculated to be 0.668 Å. So, the Co^{2+} ionic radius (0.745 Å) is larger than the

Table 1
Refined structural parameters of $La_{0.9}Te_{0.1}Mn_{1-x}Co_xO_3$ ($0\leq x\leq 0.25$) at the room temperature

Parameter	$x=0$	$x=0.05$	$x=0.10$	$x=0.15$	$x=0.20$	$x=0.25$
a (Å)	5.476	5.482	5.490	5.495	5.512	2.523
b (Å)	5.476	5.482	5.490	5.495	5.508	5.512
c (Å)	13.228	13.221	13.214	13.115	7.782	7.784
V (Å^3)	343.52	344.09	344.91	339.98	236.26	236.97
Mn–O1 (Å)					2.000	2.010
Mn–O2 (Å)					2.05	2.021
Mn–O2 (Å)					1.833	1.831
Mn–O(Å)	1.959	1.961	1.966	1.970	1.961	1.954
Mn–O1–Mn(°)					153.26	152.31
Mn–O2–Mn(°)					162.16	162.85
(Mn–O–Mn) (°)	159.09	159.06	159.05	158.89	159.19	159.45
R_p(%)	8.66	8.82	8.29	7.63	6.59	8.48

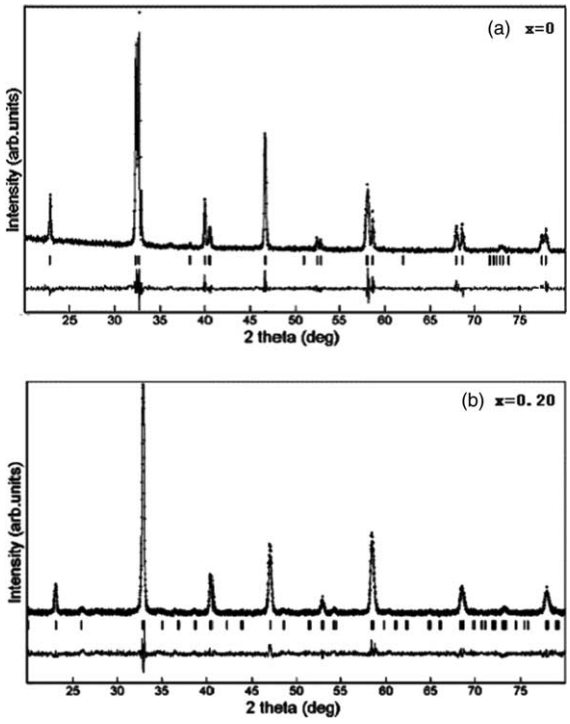

Fig. 1. XRD patterns of $La_{0.9}Te_{0.1}Mn_{1-x}Co_xO_3$ compounds, (a) $x=0$ and (b) $x=0.20$. Crosses indicate the experimental data and the calculated data is the continuous line overlapping them. The lowest curve shows the difference between experimental and calculated patterns. The vertical bars indicate the expected reflection positions.

average radius of Mn ion R(Mn_{av}), but the Co^{3+} ionic radius (0.61 Å) is smaller than the average radius of Mn ion R(Mn_{av}). Therefore, the Co^{2+} ions compress the neighboring Mn–O–Mn bonds and the Co^{3+} ions stretch the neighboring Mn–O–Mn bonds. Thus, Co exists in the form of Co^{2+} in these samples with $0\leq x\leq 0.15$. With the further increase of Co, Co^{3+} ion begins to appear and increase. It is accordance with the idea that the Co enters manganites at low doping preferably as Co^{2+} ion, and with increasing Co doping level Co^{3+} ion appears and increases. In fact, Co doping at Mn site is very complicated. Some Co^{3+} ions may appear in the samples with $0\leq x\leq 0.15$ and some Co^{2+} ions may exist in the samples with $0.20\leq x\leq 0.25$, which will be discussed below further. Therefore, with Co doping, the B-site ionic radius increases firstly and then decreases, thereby, the tolerance factor t decreases and increases correspondingly. Thus, with increasing Co doping level, the crystal structure transition from rhombohedra ($R\bar{3}C$) to orthorhombic ($Pbnm$) occurs in the electron-doped $La_{0.9}Te_{0.1}Mn_{1-x}Co_xO_3$ ($0\leq x\leq 0.25$). In addition, the disorder distribution of Mn and Co ions with Co doping is also attributed to the crystal structure transition as reported in the $LaMn_{1-x}Co_xO_3$ and the hole-doped manganites $La_{0.7}Ba_{0.3}Mn_{1-x}Co_xO_3$ samples [19].

The temperature dependence of the magnetization M of $La_{0.9}Te_{0.1}Mn_{1-x}Co_xO_3$ ($0\leq x\leq 0.25$) under both zero-field-cooling (ZFC) and filed-cooling (FC) modes at $H=0.05$ T is measured. ZFC curves are not coincide with FC ones for all samples except for the samples with $x=0$ and 0.05. FC curves for all samples are shown in Fig. 2, moreover, ZFC and FC

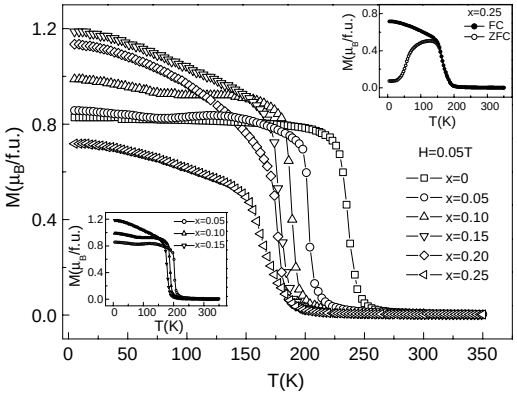

Fig. 2. Temperature dependence of magnetization for $La_{0.9}Te_{0.1}Mn_{1-x}Co_xO_3$ ($0\leq x\leq 0.25$) measured at $H=0.05$ T under the measuring mode of field cooling. M vs T for $x=0.25$ under the measuring modes of zero field cooling and field cooling is shown in the upper inset, and M vs T is shown in lower inset of Fig. 2 for the samples with $x=0.05$,0.10, and 0.15.

curves for the sample with $x=0.25$ are also presented in the upper inset of Fig. 2. It can be observed that all samples exhibit a paramagnetic (PM)–FM transition. The Curie temperatures T_C (defined as the one corresponding to the peak of dM/dT in the M vs T curve) is 238, 204, 189, 177, 176, and 160 K for $x=$ 0, 0.05, 0.10, 0.15, 0.20, and 0.25, respectively, as listed in Table 2. It can be seen that the Co doping drives T_C to lower temperatures. Although T_C decreases monotonously with increasing Co-doping level, the magnetization magnitude of Co-doping samples increases at low temperatures with increasing Co-doping level as $x\leq 0.15$, and it decreases with increasing Co-doping content further as seen from M–T curves.

It is noteworthy that T_C shows a rapid drop with a small amount of doping level (from 238 K for undoped $La_{0.9}Te_{0.1}MnO_3$ to 204 K for the doped level $x=0.05$). However, the $M(T)$ curve for the $x=0.05$ sample is rather similar to that of the undoped $La_{0.9}Te_{0.1}MnO_3$, i.e. they both show a sharp transition from PM to FM. For $x\geq 0.10$, the PM–FM phase transition becomes broader with increasing Co doping level implying the appearance of magnetic inhomogeneity. Here, we intently present the M–T curves for these samples with $x=$ 0.05, 0.10, and 0.15 as shown in the lower inset of Fig. 2. This kind of magnetic inhomogeneity is also shown by an obvious deviation between the FC and ZFC magnetization curves at low temperatures for these samples with $x\geq 0.10$. The FC and ZFC curves of the sample with $x=0.25$ are shown in the upper inset of Fig. 2. The phenomenon of the discrepancy between FC and ZFC magnetization curves is usually ascribed to the appearance of the spin glass (SG) or cluster glass (CG) induced

Table 2
Magnetic parameters of $La_{0.9}Te_{0.1}Mn_{1-x}Co_xO_3$ ($0\leq x\leq 0.25$)

Parameter	$x=0$	$x=0.05$	$x=0.10$	$x=0.15$	$x=0.20$	$x=0.25$
T_C (K)	238	204	189	177	176	160
Θ (K)	240	213	207	200	193	191
$\mu_{eff}^{Co2+}(\mu_B)$	5.01	4.91	4.81	4.72	4.63	4.53
$\mu_{eff}^{Co3+}(\mu_B)$	5.01	4.75	4.51	4.26	4.02	3.77
$\mu_{eff}^{exp}(\mu_B)$	4.93	4.90	4.72	4.53	4.11	3.80

by the competing interaction between FM and antiferromagnetic (AFM) exchange interaction. As discussed above, Co^{2+} and Co^{3+} ions are introduced by Co doping. Moreover, Mn^{4+} ion is also introduced through a CR process as in the $LaMn_{1-x}Co_xO_3$ and the hole-doped manganites $La_{0.7}Ba_{0.3}Mn_{1-x}Co_xO_3$ [19]. Therefore, there exist FM exchange interactions of Mn^{2+}–O–Mn^{3+}, Mn^{3+}–O–Mn^{4+}, and Co^{2+}–O–Mn^{4+} and AFM exchange interactions of Mn^{4+}–O–Mn^{4+}, Co^{2+}–O–Co^{2+}, Co^{2+}–O–Mn^{3+}, and Co^{3+}–O–Co^{3+} in our studied samples. In addition, the superexchange FM interaction (which will be discussed below) between Mn ions is also a factor for the formation of SG or CG. The above two kinds of magnetic interactions compete with each other, and this competition leads to the appearance of the magnetic inhomogeneity for the samples with $x \geq 0.10$.

The effect of Co doping on magnetic properties is also revealed by their field dependence of magnetization $M(H)$ from 0 to 4.5 T at $T=5$ K as shown in Fig. 3. It can be observed that, for these samples with $x=0$ and 0.05, the magnetization first increase rapidly, then reaches saturation at about 1 T and keeps constant up to 4.5 T, which is considered as a result of the rotation of the magnetic domain under external magnetic field. However, for $x=0.10$, 0.15, 0.20 and 0.25 samples, the magnetization always increases with the external magnetic field and does not reach saturation even up to a field of 4.5 T, which indicates the existence of AFM phase. That is to say, these samples have one phase separated (AFM and FM) ground state. It is well known that the competition between FM and AFM phase would lead to the appearance of SG or CG states. This is why SG or CG behavior occurs in these samples with $x \geq 0.10$. Additionally, similar to the result shown in Fig. 2, the magnetization magnitude of these Co-doping samples increases initially for $x \leq 0.15$ and then decreases with increasing Co-doping content further. Two factors are related to the very interesting phenomenon. Firstly, according to the discussion of Park et al., [10] the FM phase in $La(Mn_{1-x}Co_x)O_3$ is attributed to the FM interactions of Mn^{3+}–O–Mn^{4+} and Co^{2+}–O–Mn^{4+}. Similarly, there exist FM interactions of Mn^{3+}–O–Mn^{4+} and Co^{2+}–O–Mn^{4+} in our current Co-doping samples because Co^{2+} and Mn^{4+} ions are introduced. Therefore, we suggest that the new FM exchange interactions of Mn^{3+}–O–Mn^{4+} and Co^{2+}–O–Mn^{4+} are possible factors for the increase of magnetization at low temperatures. Secondly, from the XRD data, we can find that there is an obvious deviation of 180°of Mn–O–Mn bond angle which leads to the appearance of superexchange ferromagnetism (SFM) as discussed in Ref. [23]. The SFM phase is in fact a FM phase with predominant superexchange FM interaction. As Goodenough predicts, a Mn–O–Mn 180° superexchange interaction generally gives rise to AFM order while 90° superexchange interaction leads to FM ordering [24]. This SFM interaction has been suggested to explain FM of $Tl_2Mn_2O_7$, in which there is no Mn mixed valence [25]. The above two factors lead to the increase of magnetization with increasing the doping level for $x \leq 0.15$. However, CR process decreases the Mn^{3+} concentration, and then the CR process is slow downed correspondingly, which results in an increase of Co^{3+}/Co^{2+} ratio for further increase of x. That is to say, Co ion is divalent state for low Co doping level and it is a divalent mixed with a certain amount of trivalent for high Co doping level. Due to the decrease of Co^{2+} ions, the FM interaction of Co^{2+}–O–Mn^{4+} and Mn^{3+}–O–Mn^{4+} is weakened and the AFM interaction of Co^{3+}–O–Co^{3+} is thus strengthened, which leads to the decrease of magnetization with increasing the doping level as $x \geq 0.20$. In addition, as discussed above, the structure occurs phase transition from $R\bar{3}C$ to $Pbnm$ with these samples with $x \geq 0.20$. It is believed that the structure transition also attributes to the decrease of magnetization with these samples with $x \geq 0.20$.

Fig. 4 shows the temperature dependence of the inverse magnetic susceptibility χ_m for all samples. For a ferromagent, it is well know that, in the PM region, the relation between χ_m and the temperature T should follow the Curie–Weiss law, i.e. $\chi_m = C/(T-\Theta)$, where C is the Curie constant, and Θ is the Weiss temperature. These lines shown in Fig. 4 are the fitted curves based on the Curie–Weiss equation. It can be seen from Fig. 4 that the experimental curves in the whole PM temperature range are well described by the Curie–Weiss law. The Weiss temperature Θ is obtained to be 240, 213, 207, 200, 193 and 191 K for these samples with $x=0$, 0.05, 0.10, 0.15, 0.20 and 0.25, respectively, as listed in Table 2. For these samples with $x=0$ and 0.05, Θ almost approach their

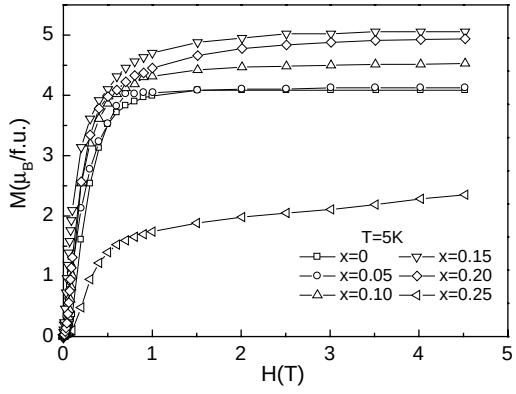

Fig. 3. Field dependence of the magnetization $M(H)$ for the compound $La_{0.9}Te_{0.1}Mn_{1-x}Co_xO_3$ ($0 \leq x \leq 0.25$) at 5 K.

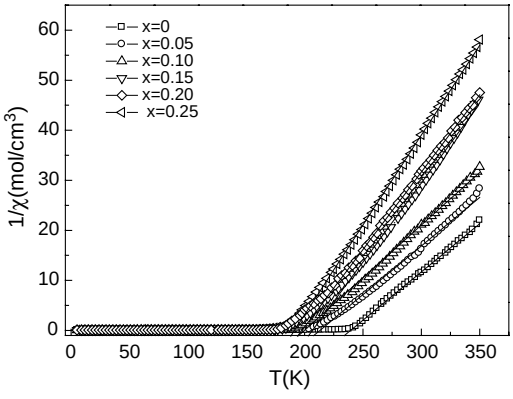

Fig. 4. Temperature dependence of the inverse of the magnetic susceptibility for $La_{0.9}Te_{0.1}Mn_{1-x}Co_xO_3$ ($0 \leq x \leq 0.25$) samples. The lines are the calculated curves according to the Curie–Weiss law.

corresponding T_C. However, for these samples with $x=0.10$, 0.15, 0.20, and 0.25, Θ are higher than the corresponding T_C, which may be related to the magnetic inhomogeneity as discussed above. And the effective magnetic moment μ_{eff} is obtained as 4.93, 4.90, 4.72, 4.35, 4.11, and 3.80 μ_B for these samples with $x=0$, 0.05, 0.10, 0.15, 0.20, and 0.25, respectively.

In the current samples, if Co always exists in form of Co^{2+}, we refer to μ_{eff} as μ_{eff}^{Co2+}. Correspondingly, if Co always exists in form of Co^{3+}, we refer to μ_{eff} as μ_{eff}^{Co3+}. We present these values in Table 2. At the same time, for the experimental μ_{eff}, it is referred to as μ_{eff}^{exp}. μ_{eff}^{exp}, μ_{eff}^{Co2+}, and μ_{eff}^{Co3+} as a function of the doping level x are plotted in Fig. 5. From this figure, one can find that for the low doping samples with $x=0$, 0.05, 0.10, and 0.15, μ_{eff}^{exp} values agree better with the data obtained from μ_{eff}^{Co2+} than those from μ_{eff}^{Co3+}, while for these samples with $x=0.20$ and 0.25, μ_{eff}^{exp} match the data obtained from μ_{eff}^{Co3+} better than those from μ_{eff}^{Co2+}. However, neither μ_{eff}^{Co2+} nor μ_{eff}^{Co3+} values equal completely with μ_{eff}^{exp} values. That is to say, in the low doping level, Co ions exist in form of Co^{2+}, with increasing Co doping level, Co^{3+} ions gradually appear and increase further. These are also accordance with these results deduced from the XRD data. At $x=0.15$, there exists a turning point in the μ_{eff}^{exp} curve as shown in this figure, which may be related to the occurrence of the structural transition.

Compared with the Cu doping in the electron-doped manganites $La_{0.85}Te_{0.15}Mn_{1-x}Cu_xO_3$ [26], the influences of FM DE interaction Mn–O–Mn of the Co doping in the electron-doped manganites $La_{0.9}Te_{0.1}Mn_{1-x}Co_xO_3$ are more complicate. The Cu ion always exists in form of Cu^{2+} within the whole doping region in $La_{0.85}Te_{0.15}Mn_{1-x}Cu_xO_3$ [26], moreover, Cu^{2+} ions do not take part in the magnetic interaction. There exist two interactions in the $La_{0.85}Te_{0.15}Mn_{1-x}Cu_xO_3$ compound. One is the Mn^{2+}–O–Mn^{3+} and Mn^{3+}–O–Mn^{4+} FM DE interaction, and the other is Mn–O–Mn SFM interaction. However, for the Co doping in the electron-doped manganites $La_{0.9}Te_{0.1}Mn_{1-x}Co_xO_3$, as discussed above, Co ions exist in form of Co^{2+} in the low doping level and Co^{3+} ions gradually appear and increase with increasing Co doping level, and both kinds of Co ions take part in the magnetic interaction. Besides the FM interaction of Mn^{2+}–O–Mn^{3+} in our current Co-doping samples, two other FM interactions of Co^{2+}–O–Mn^{4+} and Mn^{3+}–O–Mn^{4+} are also introduced due to Co doping. In addition, with increasing Co doping level, Co^{3+} ions appear and further induce the Co^{3+}–O–Co^{3+} AFM interaction.

The resistivity as a function of the temperature for $La_{0.9}Te_{0.1}Mn_{1-x}Co_xO_3$ ($0\le x\le 0.25$) is shown in Fig. 6(a) and (b). For the sample with $x=0$, there exists metal–insulator (M–I) transition at T_{P1} (=240 K), which is very close to its T_C (=238 K). In addition, there exists another M–I transition at T_{P2} (=192 K) below T_C. J. Yang et al. also reported the double-peak phenomenon in the sample $La_{0.9}Te_{0.1}MnO_3$ in Ref. [23]. It is believed to be ascribed to the coexistence of FM insulating and FM metallic phases below T_C. Upon Co doping, the M–I transition disappears and the $\rho(T)$ displays the semiconducting behavior within the entire measurement temperature range. In addition, the resistivity ρ increases with increasing Co-doping level. For the case of $x\ge 0.15$, the resistivity at low temperatures is so high that the data are collected merely in a limited temperature range because of the limitation of measuring range. It is suggested that, with increasing Co-doping level, both the increase of ρ and the disappearance of M–I transition originate from the combined effects of the destruction of Mn^{2+}–O–Mn^{3+} DE interaction network and the appearance of SFM insulating and AFM phases. This combined effects result in the carrier localization although the sample keeps up FM property. Generally speaking, both FM and metallic conduction must coexist within the framework of the DE model. However, in our current samples, the FM order is of the character of short range. FM metal phases are disconnected because of the existence of insulating phases among them, which leads to the semiconducting-like conduction behavior observed in these Co-doped

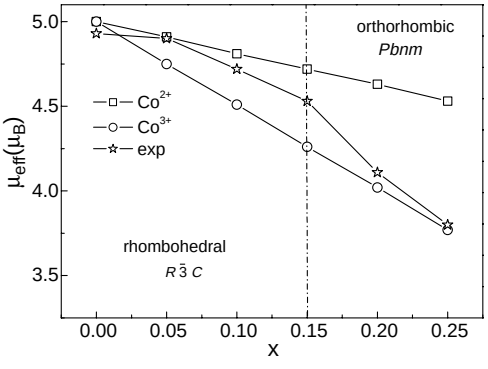

Fig. 5. Variation of the effective magnetic moment with x and the dashed lines denote the boundaries between the difference crystal structure symmetry.

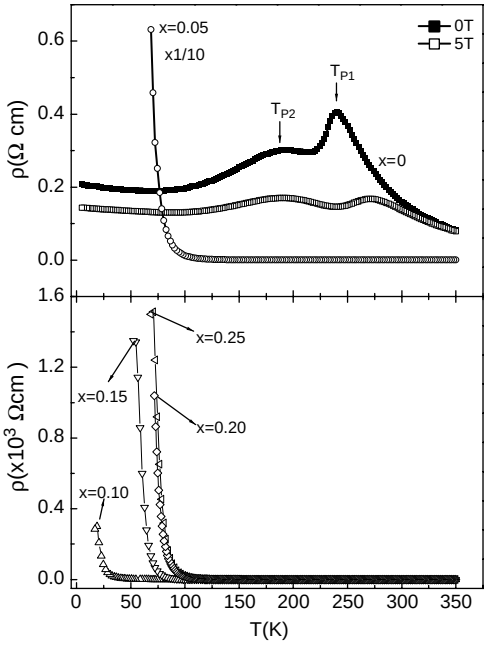

Fig. 6. Temperature dependence of the resistivity $\rho(T)$ for the compound $La_{0.9}Te_{0.1}Mn_{1-x}Co_xO_3$ ($0\le x\le 0.25$).

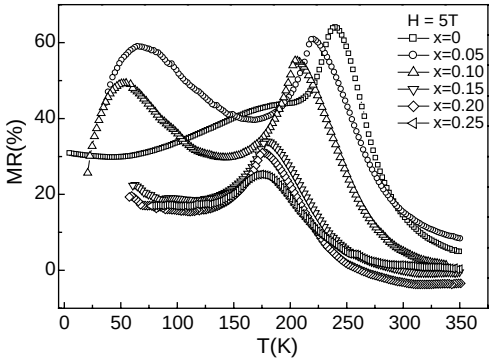

Fig. 7. Temperature dependence of magnetoresistance (MR) for the compound $La_{0.9}Te_{0.1}Mn_{1-x}Co_xO_3$ ($0 \le x \le 0.25$) at $H = 5$ T.

samples. However, compared with the effect of the Cu doping in the electron-doped manganites $La_{0.85}Te_{0.15}Mn_{1-x}Cu_xO_3$ [26], the increasing magnitude of the resistivity with the same doping content in the Co-doping $La_{0.9}Te_{0.1}Mn_{1-x}Co_xO_3$ compound is more and the disappearance trend of MIT is also quicker. The appearance of Co^{3+} and the corresponding Co^{3+}–O–Co^{3+} AFM interaction in the Co-doping $La_{0.9}Te_{0.1-}Mn_{1-x}Co_xO_3$ compound expedite the disappearance of the MIT and the increase of the resistivity. The temperature dependence of resistivity for all samples at a magnetic field of 5 T is also measured. The resistivity of the sample with $x = 0$ decreases under the applied magnetic field, the position of T_{p1} peak shifts to higher temperature and T_{P2} peak does not nearly change, as shown in Fig. 6. No obvious change of the resistivity under the applied magnetic field is observed in these Co-doped samples (no shown here).

MR as a function of temperature is presented in Fig. 7. Here the MR is defined as $\Delta\rho/\rho_H = (\rho_0 - \rho_H)/\rho_H$, where ρ_0 is the resistivity at zero field and ρ_H is the resistivity at applied magnetic field of 5 T. For the sample with $x = 0$, there exists a corresponding peak in the vicinity of T_{P1} and a small bump at T_{p2} on the MR curve. The MR behavior of these samples with $x = 0.05$ and 0.10 almost exhibits the same trend as that for $x = 0$. However, for these samples with $x = 0.15$, 0.20 and 0.25, the MR bump at low temperatures disappears and only a MR peak in the vicinity of T_C is observed. As seen from the $\rho(T)$ curves, there is no any M–I transition observed in these Co-doping samples. We suggest that the MR hump may be related to the transformation from the FM insulating phase to FM metallic phase and the connection of the FM insulating and FM metallic phase at the applied magnetic field for the samples with $x = 0$, 0.05 and 0.10. As to the disappearance of the MR hump for these samples with $x = 0.15$, 0.20 and 0.25, it may be related to their markedly enhanced SFM insulating phase and AFM interaction due to higher Co doping level.

4. Conclusion

In summary, the effect of Co-doping at Mn-site on structural, magnetic, and transport properties in the electron-doped manganites $La_{0.9}Te_{0.1}Mn_{1-x}Co_xO_3$ ($0 \le x \le 0.25$) has been investigated by measuring XRD patterns, magnetization and resistance. The room temperature structural transition from $R\bar{3}C$ to *Pbnm* symmetry is found in these samples with $x \ge 0.20$ by the Rietveld refinement of X-ray powder diffraction patterns. Co^{2+} and Mn^{4+} ions are introduced through the CR process $Mn^{3+} + Co^{3+} \rightarrow Mn^{4+} + Co^{2+}$. And with increasing the Co doping level to 0.20, some Co^{3+} ions appear and increase. The T_C values of these samples decrease with increasing the Co-doping level. The magnetization magnitude of these Co-doping samples at low temperatures increases as $x \le 0.15$ although their T_C is reduced, which is considered to be related to the appearance of the two interactions, i.e. Mn^{3+}–O–Mn^{4+} and Co^{2+}–O–Mn^{4+} FM exchange interactions and Mn–O–Mn SFM interaction. With Co doping, the M–I transition in the $x = 0$ sample is completely suppressed, which may be related to the combined effects of the destruction of Mn^{2+}–O–Mn^{3+} DE interaction network, and the appearance of SFM insulating and AFM phases due to Co doping. The difference between the Co doping and Cu doping in the Mn site in electron-doped manganites is attributed to the different valence state between Co and Mn ion and the participation of Co ions in the Mn–O–Mn interaction.

Acknowledgements

This work was supported by the National Key Research under contract No.001CB610604, and the National Nature Science Foundation of China under contract No.10474100, 10374033, and the Fundamental Bureau of the Chinese Academy of Sciences.

References

[1] R. Von Helmolt, et al., Phys. Rev. Lett. 71 (1993) 2331.
[2] S. Jin, et al., Science 264 (1994) 413.
[3] J.M. Coey, et al., Adv. Phys. 48 (1999) 167.
[4] M.B. Salamon, et al., Rev. Mod. Phys. 73 (2001) 583.
[5] P. Mandal, et al., Phys. Rev. B 56 (1997) 15073.
[6] P. Raychaudhuri, et al., J. Appl. Phys. 86 (1999) 5718.
[7] S. Roy, et al., J. Appl. Phys. 89 (2001) 7425.
[8] G.T. Tan, et al., J. Appl. Phys. 93 (2003) 5480.
[9] G.T. Tan, et al., Phys. Rev. B 68 (2003) 014426.
[10] (a) J.-H. Park, et al., Phys. Rev. B 55 (1997) 11072;
(b) C. Yaicle, et al., J. Solid State Chem. 178 (2005) 1652.
[11] Y. Sun, et al., Appl. Phys. Lett. 77 (2000) 2734.
[12] J. Blasco, et al., Phys. Rev. B 55 (1997) 8905.
[13] N. Gayathri, et al., Phys. Rev. B 56 (1997) 1345.
[14] (a) M. Miclau, et al., J. Solid State Chem. 178 (2005) 1104;
(b) M. Rubinstein, et al., J. Appl. Phys. 81 (1997) 4974.
[15] V.G. Sathey, et al., J. Phys.: Condens. Matter 10 (1998) 4045.
[16] G. Blasse, J. Phys. Chem. Solids 26 (1965) 1969.
[17] J.B. Goodenough, et al., Phys. Rev. 124 (1961) 373.
[18] G.H. Jonker, J. Appl. Phys. 37 (1966) 1424.
[19] (a) C.L. Chang, et al., J. Magn. Magn. Mater. 209 (2000) 240–242;
(b) M.F. Tai, et al., J. Magn. Magn. Mater. 209 (2000) 148–150.
[20] O. Toulemonde, et al., Solid State Commun. 118 (2000) 107.
[21] M. Sonobe, et al., J. Phys. Soc. Jpn. 61 (1992) 4193.
[22] D.B. Wiles, et al., J. Appl. Crystallogr. 14 (1981) 149.
[23] J. Yang, et al., Phys. Rev. B 70 (2004) 092504.
[24] J.B. Goodenough, Magnetism and the Chemical Bond, Interscience, New York, 1963.
[25] M.A. Subaramanian, et al., Science 273 (1996) 81.
[26] J. Yang, et al., Phys. Rev. B 70 (2005) 144421.